Mott-insulator state of cold atoms in tilted optical lattices: Doublon dynamics and multilevel Landau-Zener tunneling

Andrey R. Kolovsky[1,2] and Dmitrii N. Maksimov[1]
[1]*Kirensky Institute of Physics, Federal Research Center KSC SB RAS, 660036 Krasnoyarsk, Russia*
[2]*Siberian Federal University, 660041 Krasnoyarsk, Russia*
(Received 11 August 2016; published 14 October 2016)

We discuss the dynamical response of strongly interacting Bose atoms in an adiabatically tilted optical lattice. The analysis is performed in terms of the multilevel Landau-Zener tunneling. Different regimes of tunneling are identified and analytical expressions for the doublon number, which is the quantity measured in laboratory experiments, are derived.

DOI: 10.1103/PhysRevA.94.043630

I. INTRODUCTION

Experimental demonstration of the Mott insulator (MI) with cold atoms in 2002 [1] sparkled the interest in the controlled excitation of this highly correlated many-body state. One of the possible techniques to achieve such an excitation is the application of a lattice tilt corresponding to a static potential with uniform gradient. The major theoretical breakthrough is credited to Sachdev, Sengupta, and Girvin [2] who mapped the tilted Bose-Hubbard model with integer filling factor onto an effective Ising spin system to demonstrate that the MI state evolves to the density-wave (DW) state as the growing potential gradient traverses the point of quantum phase transition. The DW state is an ordered particle-hole excitation of the MI state in which empty lattice sites alternate with doubly occupied ones. Later on competing DW orders in a one-dimensional hard-boson model were described [3] and theoretical approaches were developed for both quench [4,5] and adiabatic [6] dynamics across the quantum critical point. The quantum phase transition predicted in Ref. [2] was confirmed in the pioneering experiment of Simons *et al.* [7] in 2011 and later in a more clear form in the experiment of Meinert *et al.* [8], where a considerable reduction of the residual harmonic confinement was achieved.

The mentioned theoretical and experimental works brought up a new trend in physics of cold atoms [9] and initiated extensive studies on a tilted Bose-Hubbard model including doublon production through dielectric breakdown [10,11], MI dynamics in parabolic confinement [12], photon-assisted tunneling for strongly correlated Bose gas [13,14], the impact of quantum quench on Bloch oscillations [15,16], upward propagation in the gravity field [17], long-range tunneling [18,19], and formation of quantum carpets [20]. Spin analogies for various involved configurations of lattice and/or interparticle interactions were proposed [21,22]. Finally, nonequilibrium dynamics of the MI state in relation to the effective Ising model was considered [23,24] where the defect density and order parameter correlation function were computed. Recent progress in the field of out-of-equilibrium dynamics in strongly interacting one-dimensional systems is reviewed in Ref. [25] while the numerical techniques for solving the Bose-Hubbard model with a tilt are addressed in Ref. [26].

In this paper we approach the problem from a different viewpoint. Namely, instead of mapping the bosonic system into a spin system, we employ the theory of multilevel Landau-Zener (LZ) tunneling. This theory is an extension of the common Landau-Zener theory from two onto many (including the case of infinitely many) levels, showing a structured avoided crossing [27–31]. We identify the diabatic and adiabatic regimes of the multilevel LZ tunneling and derive asymptotic equations for the number of produced doublons depending on the system parameters. Importantly, our approach admits a straightforward generalization onto two-dimensional tilted lattices, which have so far attracted less attention.

II. THE MODEL AND MAIN EQUATIONS

First we discuss the one-dimensional case. We consider a unit-filled Bose-Hubbard model with the following Hamiltonian:

$$\widehat{H} = -\frac{J}{2}\sum_l (\hat{a}^\dagger_{l+1}\hat{a}_l + \text{H.c.}) + \frac{U}{2}\sum_l \hat{n}_l(\hat{n}_l - 1) + F\sum_l l\hat{n}_l, \tag{1}$$

where J is the hopping matrix element, U is the microscopic interaction constant, and the external field $F = F(t)$ is assumed to slowly increase from zero to a value above the interaction constant U. Throughout the paper we use the periodic boundary condition, which can be imposed after applying the gauge transformation for the external field. Thus we simulate the dynamics of the following system,

$$\widehat{H}(t) = -\frac{J}{2}\sum_{l=1}^{L}(\hat{a}^\dagger_{l+1}\hat{a}_l e^{i\theta(t)} + \text{H.c.}) + \frac{U}{2}\sum_{l=1}^{L}\hat{n}_l(\hat{n}_l - 1), \tag{2}$$

where $\theta(t) = \int_0^t F(t')dt'$ and $\hat{a}_{L+1} \equiv \hat{a}_l$. The periodic boundary condition facilitates the study of the thermodynamic limit $N = L \to \infty$. Going ahead, we mention that convergence of the results towards the thermodynamic limit crucially depends on the sweeping rate $\nu = dF/dt$, which is our control parameter. We found rapid convergence for large ν, while it was asymptotically slow if $\nu \to 0$.

Next we comment on the Hilbert space of the Hamiltonian (2). For the unit filling factor the whole Hilbert space of L bosons can be truncated to the subspace spanned by the Fock

states $|\mathbf{n}\rangle = |n_1,n_2,\ldots,n_L\rangle$, where the number of atoms in a given site can be 0, 1, or 2. Accuracy of this approximation is mainly controlled by the ration J/U, which we choose to be <0.1. We mention, however, that in some cases the condition $J/U \ll 1$ is not sufficient and the validity of the above approximation should be checked independently by simulating the system dynamics in the whole Hilbert space [32]. We come back to this point in Sec. V.

The discussed subspace is reduced further by noticing that the periodic boundary condition conserves the total quasimomentum κ. Thus, the Hamiltonian matrix can be split into L blocks by introducing the translationally invariant Fock states. We are interested only in the $\kappa = 0$ block because it contains the initial MI state. In what follows we refer to the specified Hilbert space as the *doublon Hilbert space* and denote its dimension by $\mathcal{N}_D$. Two states of our prime interest in this Hilbert space are the MI state

$$|MI\rangle = |1,1,1,1,\ldots\rangle$$

and the DW state

$$|DW\rangle = \frac{1}{\sqrt{2}}(|0,2,0,2,\ldots\rangle + |2,0,2,0,\ldots\rangle)\,, \qquad (3)$$

where the symmetric form of the DW state is obviously due to the periodic boundary condition.

Finally we introduce the instantaneous Floquet operator which is at the core of our analytical approach. To calculate this operator we fix F, so that $\theta(t) = Ft$ in Eq. (2), and calculate the evolution operator over the Bloch period $T = 2\pi/F$,

$$\widehat{W} = \widehat{\exp}\left(-i\int_0^T \widehat{H}(t)dt\right), \qquad (4)$$

where the hat over the exponent sign denotes the time ordering. Let us briefly discuss the spectrum of the operator (4). It is convenient to begin with the case of zero hopping where the Fock states $|\mathbf{n}\rangle$ are also eigenstates of the Floquet operator:

$$\widehat{W}|\mathbf{n}\rangle = \lambda|\mathbf{n}\rangle, \quad \lambda = \exp\left(-i\frac{\pi U}{F}\sum_{l=1}^{L} n_l(n_l-1)\right). \qquad (5)$$

Plotting eigenphases $\mathrm{angle}(\lambda) = i\log(\lambda)$ as the function of $1/F$ we obtain a characteristic pattern shown in Fig. 1(a). Each line in this figure is associated with a fixed number of doublons: the line with zero slope is the MI state, the first line with nonzero slope represents the one-doublon states, etc., and the line with the maximal slope is the DW state.

For $J = 0$ the majority of levels in Fig. 1(a) are multiply degenerate, with the MI and DW states being obvious exclusions. Nonzero J removes the degeneracy and originates the multilevel avoided crossings at $F = U/j$, where j is a positive integer number [see Fig. 1(b)]. These avoided crossings are associated with the first-order ($j = 1$), second-order ($j = 2$), etc., resonant tunneling of atoms in the tilted lattice. Our ultimate goal is to calculate the number of doublons N_d as we subsequently traverse the multilevel avoided crossings in Fig. 1(b) by tilting the lattice from $F = 0$ to $F > U$. For the purpose of future discussions Fig. 2(a) shows $N_d = N_d(t)$, which is obtained by the straightforward numerical simulations of time evolution of the system (2), where we used the linear ramp for the static field, i.e., $F/U = \nu t$ [and, hence, $\theta(t) = U\nu t^2/2$]. For a large sweeping rate N_d is seen to approach zero while for a small ν it evolves in a stepwise manner, where the positions of the steps correlate with positions of the avoided crossings in Fig. 1(b).

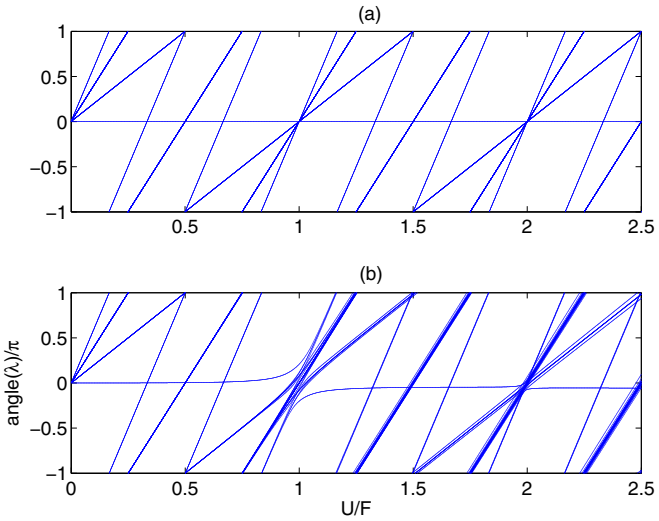

FIG. 1. Spectrum of the Floquet operator (4) as the function of U/F for $J = 0$ (a) and $J = 0.04U$ (b). The system size $L = 6$, where the dimension of the doublon Hilbert space $\mathcal{N}_D = 26$.

III. MULTILEVEL LANDAU-ZENER TUNNELING

We analyze each multilevel avoided crossing (MLAC) separately. It is instructive to begin with the case $j = 1$ which corresponds to the first-order resonant tunneling.

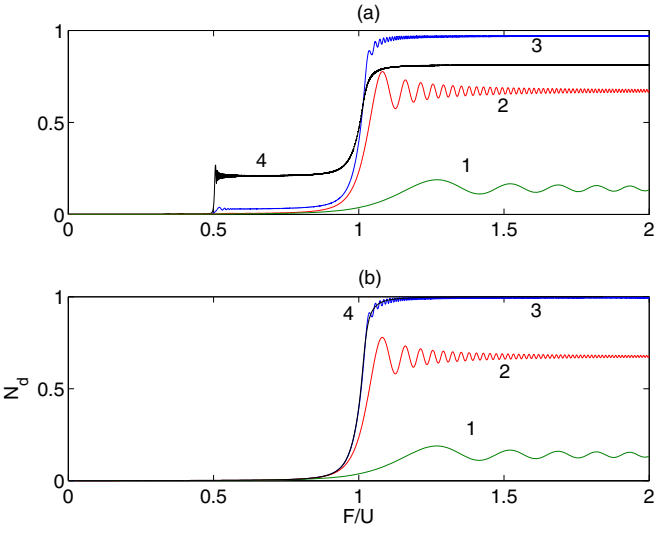

FIG. 2. The mean number of doublons N_d normalized to $N_{\max} = L/2$ as the function of time for different sweeping rates ν, calculated by using the doublon Hilbert space (a) and $j = 1$ resonant subspace (b). The parameters are $J = 0.02U$, $L = 6$, and $\nu = 10^{-1}/2\pi$ (marked by 1), $\nu = 10^{-2}/2\pi$ (marked by 2), $\nu = 10^{-3}/2\pi$ (marked by 3), and $\nu = 10^{-4}/2\pi$ (marked by 4). The time is related to F as $F/U = \nu t$.

A. The case $j = 1$

The first step in the analysis is to identified the *resonant subspace*. In the case $j = 1$ the resonant subspace consists of doublon Fock states with the additional constraint that two doublons cannot occupy the nearest sites [2]. This constraint drastically decreases the dimension of the doublon Hilbert space through removing all irrelevant states, i.e., those that cannot be excited from the initial MI state by means of the first-order resonant tunneling. For the parameters of Fig. 1(b) the relevant states are shown in Fig. 3(a). Notice that the MI state (the horizontal line) is analytically connected with the DW state (the line with the maximal slope). An important quantity which can be extracted from the depicted spectrum is the minimal gap Δ separating the lowest level, i.e., the level which analytically connects the MI and DW states, from the next level. Since the number of levels in the MLAC progressively increases with L [see Eq. (A4) in the Appendix A] the gap Δ tends to zero as L tends to infinity and we found that with good accuracy

$$\Delta = 8J/L\ . \tag{6}$$

After truncating the doublon Hilbert space to the resonant subspace the problem can be reformulated as a problem of multilevel Landau-Zener tunneling [27–29]. This theory deals with systems of the following type,

$$i\frac{d\psi}{dt} = (H_1 + tH_2)\psi, \quad -\infty < t < \infty, \tag{7}$$

where H_1 and H_2 are two matrices or two Hamiltonians. For the currently considered case $j = 1$ these Hamiltonians were found in Refs. [2,7], where they were expressed through the spin operators of the effective spin system. In our analysis we do not use this mapping and calculate the matrices H_1 and H_2 directly from the original Hamiltonian. Given $F/U = \nu t$ the instantaneous spectrum of the effective Hamiltonian $H(t) = H_1 + tH_2$ coincides with the spectrum of the Floquet operator shown in Fig. 3(a) after folding the former into the fundamental energy interval $-F/2 \leqslant E < F/2$.

As soon as we know the matrices H_1 and H_2 we can use a number of rigorous results from the theory of multilevel LZ tunneling. Let us define the *integral* probability of LZ tunneling across the MLAC as

$$\mathcal{P}_{\rm LZ} = 1 - \frac{N_d(t=\infty)}{N_{\rm max}}, \tag{8}$$

where $N_{\rm max} = L/2$ is the maximally possible number of doublons. We mention that definition (8) differs from the standard definition of multilevel LZ tunneling which involves $\mathcal{N}_R(\mathcal{N}_R+1)/2$ transition probabilities between the instantaneous states of the system. (Here $\mathcal{N}_R$ is the dimension of the resonant subspace which determines the size of the matrices H_1 and H_2.) The advantage of Eq. (8) is that it converges in the thermodynamic limit. This allows us to use terminology of the two-level Landau-Zener problem: we call transition across the MLAC diabatic if $\mathcal{P}_{\rm LZ} \approx 1$ and adiabatic if $\mathcal{P}_{\rm LZ} \approx 0$.

We begin with the diabatic regime. Using Eq. (13) in Ref. [28] it can be proved that in the limit of large ν the integral probability is given by

$$\mathcal{P}_{\rm LZ} = \exp\left(-\pi\frac{J^2}{\nu U}\right). \tag{9}$$

Here "large ν" means that $P_{\rm LZ}$ is close to unity. Notice that $P_{\rm LZ} \approx 1$ does not imply occupation of the MI state to be close to unity—on the contrary, in the thermodynamic limit it goes to zero. The accuracy of Eq. (9) is illustrated in the main panel in Fig. 4. In this figure the dashed line is Eq. (9) and the solid lines are numerical results for different system sizes $6 \leqslant L \leqslant 18$.

We proceed with the opposite case of small ν. Here one clearly sees the finite-size effect due to a finite gap Δ between the lowest level and the next level in Fig. 3(a). Because of the gap the system sooner or later enters the usual adiabatic regime where the probability to stay in the lowest level approaches unity while the probability to appear in the next level is an exponentially small value given by the celebrated Landau-Zener formula: $P = \exp(-\alpha\Delta^2/\nu)$, where $\alpha \sim 1$ is a constant determined by the angle between

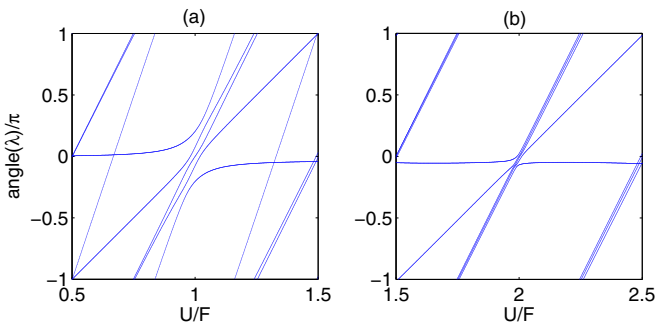

FIG. 3. MLAC at $F = U$ (a) and $F = U/2$ (b). The parameters are as follows: $L = 6$, and $J = 0.02U$ in panel (a) and $J = 0.04U$ in panel (b).

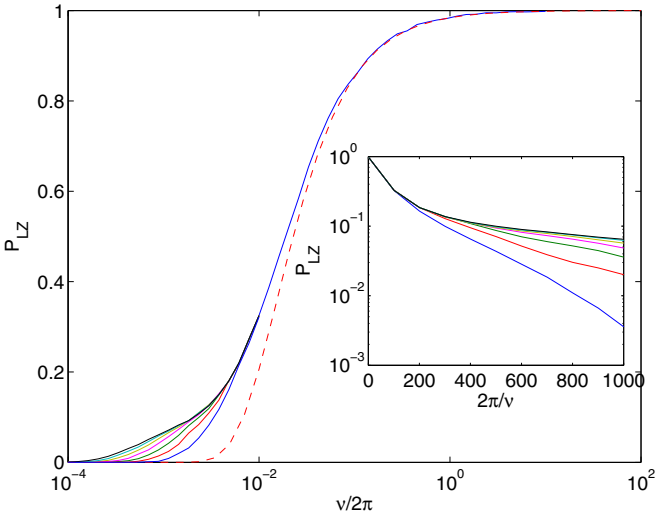

FIG. 4. Probability of LZ tunneling across the $j = 1$ MLAC as the function of the sweeping rate ν for different system sizes $L = 6$, 8, 10, 12, 14, 16, and 18. The corresponding dimensions of the resonant subspaces are $\mathcal{N}_R = 5$, 8, 15, 31, 64, 143, and 329. The hopping matrix element $J = 0.02U$. The inset shows the same data in the semilogarithmic scale as the function of $1/\nu$.

two asymptotes for the energy level positions. Thus, at the end point of the adiabatic passage one finds $N_d(t=\infty) = \frac{L}{2}(1-P) + (\frac{L}{2}-1)P$. Taking into account our definition of $\mathcal{P}_{\rm LZ}$, Eq. (8), this gives

$$\mathcal{P}_{\rm LZ} = \frac{2}{L}\exp\left(-\mathcal{C}_{\rm LZ}\frac{\Delta^2(L)}{\nu}\right), \quad \nu \to 0, \tag{10}$$

where, according to our numerical studies, $\mathcal{C}_{\rm LZ} \approx 1.7$. The asymptotic behavior (10) is exemplified in the inset in Fig. 4 which shows the logarithm of $\mathcal{P}_{\rm LZ}$ as the function of the inverse sweeping rate.

Since the gap $\Delta(L)$ in Eq. (10) vanishes in the thermodynamic limit $L \to \infty$, we obtain completely different results if the limits $\nu \to 0$ and $L \to \infty$ are exchanged. To find $\mathcal{P}_{\rm LZ}$ in this case (i.e., to find the limiting curve in Fig. 4) we proceed as follows. Assume for the moment a finite L. Then we can choose ν small enough for only two levels to be involved in the Landau-Zener dynamics. The simplest possible condition for the onset of two-level tunneling with the probability given by Eq. (10) is $\nu = \mathcal{C}_{\rm LZ}\Delta^2(L)$. Combining the above equation with the estimate (6) for the gap width Δ and Eq. (10) we can eliminate L, which gives

$$\mathcal{P}_{\rm LZ} = \frac{1}{2J}\left(\frac{\nu}{\mathcal{C}_{\rm LZ}}\right)^{\frac{1}{2}}. \tag{11}$$

The obtained algebraic dependence is in agreement with numerical results of Ref. [23] where $\mathcal{P}_{\rm LZ}$ was argued to scale as $\mathcal{P}_{\rm LZ} \sim \nu^{1/2}$ in the thermodynamic limit.

B. The case $j = 2$

In the case $j = 2$, which corresponds to the second-order resonant tunneling, the spectrum of the Floquet operator in the resonant subspace is depicted in Fig. 3(b). For the considered example the resonant subspace consists of five Fock states: the MI state $|111111\rangle$, one-doublon state, $|111012\rangle$, which is resonantly related to the MI state via the intermediate state $|111021\rangle$; two-doublon states, $|012012\rangle$ and $|110022\rangle$, which are related to the one-doublon state via the states $|021012\rangle$ and $|110112\rangle$, respectively; and the two-doublon state $|020112\rangle$, which can be obtained from the two-doublon state $|012012\rangle$ via the intermediate state $|021012\rangle$. (It is implicitly assumed that all these states are symmetrized by using cyclic permutation to satisfy the conservation law for the total quasimomentum.) To find the MLAC shown in Fig. 3(b) one first calculates the Floquet operator keeping the intermediate states and then eliminates them by projecting this operator onto the basis of the resonant states. This results in the effective Hamiltonian where the resonant states are directly related to each other by the transition matrix elements which are proportional to J^2/U. Thus we can use the results of the previous subsection with some minor modifications. First, the maximally possible doublon number $N_{\rm max} = L/3$ but not $L/2$. Second, the critical value of the sweeping rate ν which separates the diabatic and adiabatic regimes of the multilevel LZ tunneling scales as J^4 but not J^2.

IV. DYNAMICS OF DOUBLON NUMBER

In the previous section we considered different regimes of LZ tunneling across a MLAC. It was argued, in particular, that the adiabatic regime is sensitive to the system size. This result, however, is more of academic than of practical interest. In fact, in the laboratory experiment one deals with an ensemble of one-dimensional (1D) lattices where the lattice lengths are determined by the distances between defects in the initial MI state. Thus, the system size L is, strictly speaking, not known. At the same time, as it is seen in Fig. 4 an error in the dependence $\mathcal{P}_{\rm LZ} = \mathcal{P}_{\rm LZ}(\nu)$ due to unknown L never exceeds a few percent. This allows us to make reliable predictions by analyzing the lattices of a rather small size. With this in mind we address the dependence $N_d = N_d(t)$ in the limit of small ν, which is of prime experimental interest.

Let us assume the sweeping rate ν to be small enough to ensure a truly adiabatic regime. In the other words, we follow the lowest level in Fig. 3(a) which analytically connects the MI state with the DW state. Denoting by $|\Psi(F)\rangle$ the instantaneous eigenstate of the Floquet operator associated with this level we have

$$N_d(F) = \langle\Psi(F)|\hat{D}|\Psi(F)\rangle, \tag{12}$$

where $\hat{D}$ is the doublon number operator. Below we display analytical solutions of Eq. (12) for $L = 2$ and $L = 4$ and compare them with the numerical solutions for $L \to \infty$. It should be mentioned that Eq. (12) rapidly converges as L is increased and the corresponding curves become undistinguishable in the linear scale if $L \geqslant 8$.

For $L = 2$ the dimension of the resonant subspace $\mathcal{N}_R = 2$ and the problem reduces to the diagonalization of a 2×2 matrix,

$$H(F) = \begin{pmatrix} 0 & -J \\ -J & \delta(F) \end{pmatrix},$$

where $\delta(F) = U - F$. For the mean number of doublons this model gives

$$\frac{N_d(F)}{N_{\rm max}} = \frac{\left(\delta - \sqrt{\delta^2+4J^2}\right)^2}{4J^2 + \left(\delta - \sqrt{\delta^2+4J^2}\right)^2}. \tag{13}$$

Next consider $L = 4$. In this case $\mathcal{N}_R = 3$ and

$$H(F) = \begin{pmatrix} 0 & -\sqrt{2}J & 0 \\ -\sqrt{2}J & \delta(F) & -J \\ 0 & -J & 2\delta(F) \end{pmatrix}.$$

After some algebra we get

$$\frac{N_d(F)}{N_{\rm max}} = \frac{(E^2-\delta^2)^2 + 2J^2(E+\delta)^2}{2J^2(E-\delta)^2 + J^2(E+\delta)^2 + (E^2-\delta^2)^2}, \tag{14}$$

where $E = E(F)$ denotes the position of the lowest level:

$$E(F) = 2\sqrt{\frac{3J^2+\delta^2}{3}}\cos\left(\frac{\eta+2\pi}{3}\right),$$

$$\eta(F) = \pi\theta(\delta) - \arctan\left(\frac{2\sqrt{\left(\frac{3J^2+\delta^2}{3}\right)^3 - \left(\frac{J^2\delta}{2}\right)^2}}{J^2\delta}\right).$$

We found that there is no need to consider the next approximation because Eq. (14) reproduces the results for $L \to \infty$ with

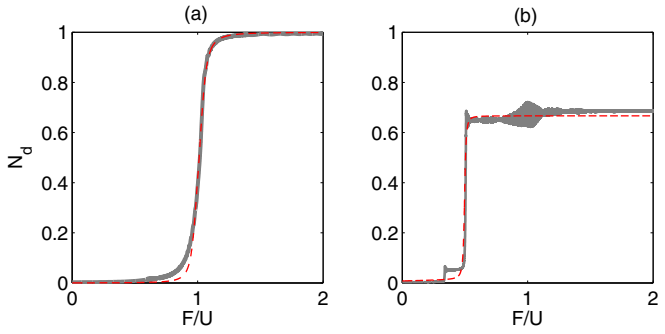

FIG. 5. Number of doublons as the function of $F = F(t)$ for two different protocols: a piecewise ramp with $\nu = 1.25 \times 10^{-2}$ in the interval $0 \leqslant F/U < 0.6$ and $\nu = 2.5 \times 10^{-4}$ in the interval $0.6 \leqslant F/U < 2$ (a), and the linear ramp in the interval $0 \leqslant F/U < 2$ with the rate $\nu = 2 \times 10^{-5}$ (b). The dashed lines are analytical results of Eqs. (14) and Eq. (B4), respectively. The system size $L = 8$, where the dimension of the doublon Hilbert space $\mathcal{N}_D = 142$. The hopping matrix element $J = 0.04U$.

accuracy higher than 1% . Thus, for practical purposes one can use Eq. (14) or, even simpler, Eq. (13). It follows from these equations that the characteristic width of the step for $N_d(F)$ is proportional to J.

A similar equation can be derived for the second-order resonant tunneling at $F = U/2$ [see Eq. (B4) in Appendix B]. The dependencies (14) and (B4) are shown in Fig. 5 by the dashed lines.

It is interesting to compare Eqs. (14) and (B4) against direct numerical simulations of the doublon dynamics (see solid lines in Fig. 5). We mention that in these simulations we use the doublon Hilbert space and, hence, no resonant approximations are involved. In Fig. 5(b) we tilt the lattice by using the linear ramp with the rate $\nu = 2 \times 10^{-5}$, which is small enough to ensure the adiabatic regime for the MLAC at $F = U/2$. In Fig. 5(a) we tilt the lattice by using a protocol with two different rates: in the interval $0 \leqslant F/U < 0.6$ the rate $\nu = 1.25 \times 10^{-2}$ is used, which ensures the diabatic regime for MLAC at $F = U/2$; in the interval $0.6 \leqslant F/U < 2$ the rate is changed to $\nu = 2.5 \times 10^{-4}$, which insures the adiabatic regime for the second avoided crossing at $F = U$. A good agreement with analytical results is noticed.

V. TWO-DIMENSIONAL LATTICES

In this section we generalize the results of the previous sections to the two-dimensional case,

$$\begin{aligned}\widehat{H} = &-\frac{J_x}{2}\sum_{l,m}(\hat{a}^\dagger_{l+1,m}\hat{a}_{l,m} + \text{H.c.}) \\ &-\frac{J_y}{2}\sum_{l,m}(\hat{a}^\dagger_{l,m}\hat{a}_{l,m+1} + \text{H.c.}) \\ &+\frac{U}{2}\sum_{l,m}\hat{n}_{l,m}(\hat{n}_{l,m} - 1) \\ &-F(t)\sum_{l,m}[l\cos\phi + m\sin\phi]\hat{n}_{l,m}\,, \qquad (15)\end{aligned}$$

where, as before, $F(t)$ changes linearly in time with the rate ν, and the initial state of the system is a Mott insulator with unit filling. Like for 1D lattices we use the periodic boundary conditions, which are imposed after applying the gauge transformation. Thus we simulate the dynamics of a finite system of the size $L_x \times L_y$ with the Hamiltonian

$$\begin{aligned}\widehat{H}(t) = &-\frac{J_x}{2}\sum_{l=1}^{L_x}\sum_{m=1}^{L_y}(\hat{a}^\dagger_{l+1,m}\hat{a}_{l,m}e^{-i\theta_x(t)} + \text{H.c.}) \\ &-\frac{J_y}{2}\sum_{l=1}^{L_x}\sum_{m=1}^{L_y}(\hat{a}^\dagger_{l,m+1}\hat{a}_{l,m}e^{-i\theta_y(t)} + \text{H.c.}) \\ &+\frac{U}{2}\sum_{l=1}^{L_x}\sum_{m=1}^{L_y}\hat{n}_{l,m}(\hat{n}_{l,m} - 1)\,, \qquad (16)\end{aligned}$$

where $\theta_x(t) = \int F_x(t)dt$ and $\theta_y(t) = \int F_y(t)dt$. The main difference and challenge of the 2D system (16) as compared to the 1D system (2) is sensitivity to the field orientation. The cases where **F** is exactly aligned or slightly misaligned with one of the primary axes of the lattice have been analyzed in the recent work [34]. Here we address another important case where **F** is *strongly* misaligned with the primary axes. It is shown below that strongly misaligned 2D lattices are closer to the one-dimensional situation than the aligned lattices.

A. Floquet operator

To be specific we consider the field orientation $F_x/F_y \approx 1/2$ and we begin with the case where $F_x/F_y = 1/2$ exactly. In this case we can introduce the Floquet operator,

$$\widehat{W} = \widehat{\exp}\left(-i\int_0^T \widehat{H}(t)dt\right), \qquad (17)$$

where $T = 2\pi/F_x = 4\pi/F_y$ is the common Bloch period. Similar to 1D tilted lattices we restrict ourselves by the doublon Hilbert space where $n_{l,m} \leqslant 2$. The validity of this, not obvious for 2D tilted lattices approximation, will be checked later on. Using the doublon Hilbert space we calculate the spectrum of the operator (17) and decompose it into $L_x \times L_y$ independent spectra according to the total quasimomentum. As before, we are bound with the zero quasimomentum subspace because the MI state belongs to this subspace. The obtained spectrum is shown in Fig. 6 for the lattice 2×4, $J_y = 0.02U$, and $J_x = 0$, panel (a), and $J_x = 0.04U$, panel (b).

Let us discuss the depicted spectra in more detail. The spectrum in Fig. 6(a) obviously reproduces the spectrum of two independent 1D lattices of the length $L = L_y$, where the MLAC at $F/U = \sqrt{5}/2$ corresponds to the first-oder tunneling in the y direction. The spectrum in Fig. 6(b) contains extra MLACs at $F/U = \sqrt{5}$, which corresponds to the first-order tunneling in the x direction, and a number of less pronounced crossings corresponding to the second-order tunneling. In what follows we focus on the first-order resonance at $F/U = \sqrt{5}/2$.

If $J_x = 0$ the doublon Hilbert space can be truncated to the resonant subspace, which is given by the tensor product of two (in general case, L_x) 1D resonant subspaces introduced earlier in Sec. III. The spectrum of the operator (17) on this subspace

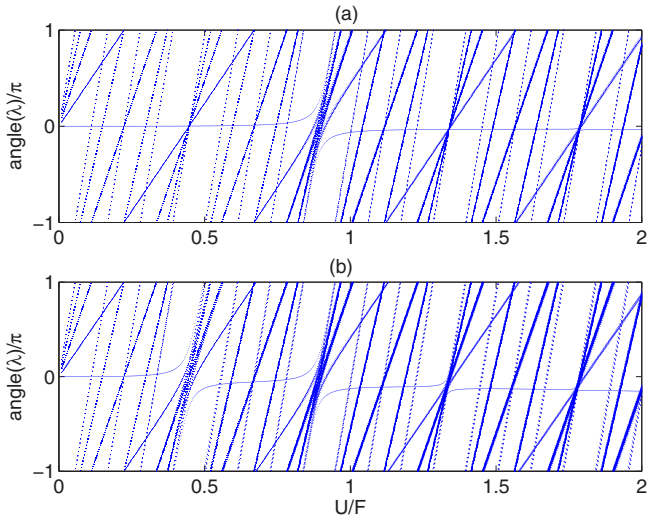

FIG. 6. Eigenphases of the Floquet operator as the function of U/F for $F_x/F_y = 1/2$ and (a) $J_x = 0$ and (b) $J_x = 0.04U$. The lattice size is 2×4 (dimension of the doublon Hilbert space $\mathcal{N}_D = 147$), and the hopping matrix element $J_y = 0.02U$.

is shown in Fig. 7(a). Our particular interest in Fig. 7(a) is the "lowest" level. Using the fact that two 1D lattices are independent it is easy to prove that this level analytically connects the MI state with the state

$$|\psi\rangle = \frac{1}{\sqrt{2}}(|\mathrm{DW}\rangle + |\widetilde{\mathrm{DW}}\rangle), \tag{18}$$

where $|\mathrm{DW}\rangle$ is the "correlated" DW state,

$$|\mathrm{DW}\rangle = \frac{1}{\sqrt{2}}\left[\begin{pmatrix}22\\00\\22\\00\end{pmatrix} + \begin{pmatrix}00\\22\\00\\22\end{pmatrix}\right], \tag{19}$$

and $|\widetilde{\mathrm{DW}}\rangle$ is the "uncorrelated" DW state,

$$|\widetilde{DW}\rangle = \frac{1}{\sqrt{2}}\left[\begin{pmatrix}20\\02\\20\\02\end{pmatrix} + \begin{pmatrix}02\\20\\02\\20\end{pmatrix}\right]. \tag{20}$$

Let now $J_x \neq 0$ and, hence, two 1D lattices are no more independent. To account for the lattice coupling we use the

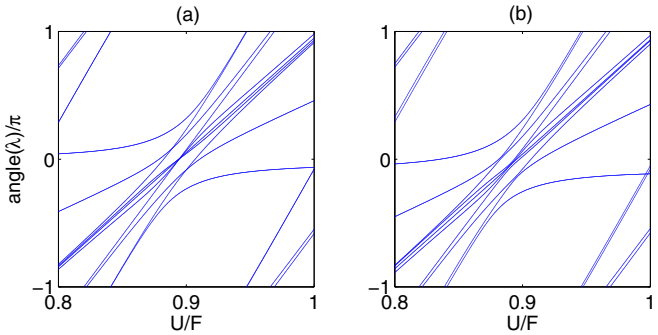

FIG. 7. The spectrum of the Floquet operator on the resonant subspace ($\mathcal{N}_R = 10$) for $J_x = 0$ (a) and $J_x = 0.04U$ (b).

specific perturbation theory in the parameter J_x. The procedure involves two steps and goes as follows. First we introduce the new basis which diagonalizes the Floquet operator (17) for $J_y = 0$. We refer to this basis as many-body Wannier-Stark states. If $J_x \ll F_x$ and $F_x \neq U$ (the latter condition ensures that there is no resonant tunneling in the x direction) these many-body Wannier-Stark states can be approximated by the Fock states which, however, have slightly different energies:

$$E_i = E_i^{(0)} + \Delta E_i\ , \quad E_i^{(0)} = \langle \mathbf{n}_i | \frac{U}{2} \sum_{l,m} \hat{n}_{l,m}(\hat{n}_{l,m} - 1) | \mathbf{n}_i \rangle . \tag{21}$$

We find the energies E_i by calculating diagonal elements of the Floquet operator for $J_y = 0$, i.e., by dropping the second term in the Hamiltonian (16). Notice that for $J_y = 0$ the system becomes quasi-one-dimensional. For this reason the above-introduced correction ΔE_i to the energy of ith Fock states can be found semianalytically by using simple combinanatorics.

In the second step we calculate the Floquet operator (17) approximately, by dropping the first term in the Hamiltonian (16) and simultaneously correcting the energies of the Fock states. This again reduces the 2D problem to a quasi-1D problem, where the x degree of freedom is now taken into account by nonzero ΔE_i. The accuracy of the method is illustrated in Fig. 8(a) which compares the eigenphases of the exact and approximate Floquet operators for $J_y = 0.02U$ and $J_x = 0.04U$.

The described approach, although perturbative, has several advantages over the straightforward diagonalization of the Floquet operator. First, it allows us to treat larger lattices by reducing the 2D problem to the sequence of two quasi-1D problems. Second, it can be also used in the case of irrational orientations of the field, where one has no common Bloch

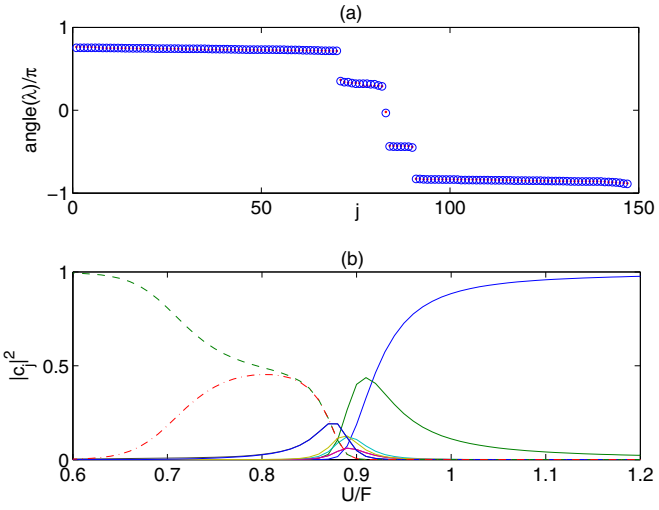

FIG. 8. (a) Exact (dots) and approximate (open circles) eigenphases of the Floquet operator for $F_x/F_y = 1/2$. The other parameters are $U/F = 0.8$, $J_y = 0.02U$, and $J_x = 0.04U$. (b) Squared modulus of the expansion coefficients c_i for the eigenstate associated with the lowest level in Fig. 7(b). The coefficients in front of the correlated and uncorrelated DW states are marked by the dashed and dash-dotted lines, respectively. The hopping matrix element J_x is set to a very small yet finite value of $J_x = 0.001U$.

period. Finally, it justifies the resonant approximation for $J_x \neq 0$ and provides a physical interpretation of the numerical results in terms of the energies ΔE_i. Figure 7(b) shows the spectrum of the Floquet operator for $J_x = 0.04U$, calculated by using the resonant Hilbert space. It is seen that the lowest level is now separated from the next level by the finite gap $\widetilde{\Delta}$. The size of the gap is given by the difference between the energy corrections ΔE_i to the correlated DW state (19) and uncorrelated DW state (20), which was found to scale as

$$\widetilde{\Delta} \approx 5J_x^2/U. \tag{22}$$

The presence of the gap also breaks the symmetry of the $J_x = 0$ problem so that the MI state is now analytically connected with the correlated DW state but not with the symmetric state (18). This is illustrated in Fig. 8(b), which shows expansion coefficients over the symmetrized Fock basis for the eigenstate $|\Psi(F)\rangle$ associated with the lowest level,

$$|\Psi(F)\rangle = \sum_{i=1}^{\mathcal{N}_R} c_i(F)|\mathbf{n}_i\rangle. \tag{23}$$

Our prime interest in this figure is the expansion coefficients in front of the correlated DW state (19), dashed line, and in front of the uncorrelated DW state (20), dash-dotted line. Notice that for $J_x = 0$ these coefficients would be equal, so that the dashed and dashed-dotted line would approach $1/2$ in Fig. 8(b). However, when $J_x \neq 0$ the coefficient in front of the uncorrelated DW state is seen to vanish while the coefficient in front of the correlated DW state tends to unity. This means that in the deep adiabatic regime the final state of the system is the correlated DW. This result holds for arbitrary L_x where we have several uncorrelated DW states. For example, for $L_x = 4$ these are

$$\begin{pmatrix}2220\\0002\\2220\\0002\end{pmatrix}, \quad \begin{pmatrix}2200\\0022\\2200\\0022\end{pmatrix}, \quad \begin{pmatrix}2020\\0202\\2020\\0202\end{pmatrix}. \tag{24}$$

[Unlike Eqs. (19) and (20) here we display not symmetrized Fock states—the symmetrization procedure is assumed implicitly.] We found that the closest to the energy of the correlated DW state is the uncorrelated DW state which is obtained from the former by shifting one column, like the first state in Eq. (24). Furthermore, the energy difference between these two states (i.e., the difference between associated corrections ΔE_i) is essentially independent of L_x. Thus, the correlated DW state is separated from a bundle of uncorrelated DW states by a finite gap, where Eq. (22) provides an estimate for the gap size.

B. Dynamics of doublon number

This subsection presents numerical solutions of the time-dependent Schrödinger equation with the Hamiltonian (16) where $F(t) = \nu t$. Simulations are performed in the doublon Hilbert space. Figure 9(c) shows the doublon number N_d as the function of time for the lattice 2×4 and $\nu = 10^{-3}/2\pi$. As expected, one finds many similarities with Fig. 2(a) showing the result for 1D lattices. In particular, small steps are due to the second-order tunneling and the large step at $F/U = \sqrt{5}/2$ is due to the first-order tunneling. By using an appropriate protocol for the sweeping rate ν we can ensure the diabatic regime for MLACs associated with the second-order tunneling. Then the main step is described by Eq. (14) and $N_d(t)$ approaches $N_{\max} = L_x L_y/2$.

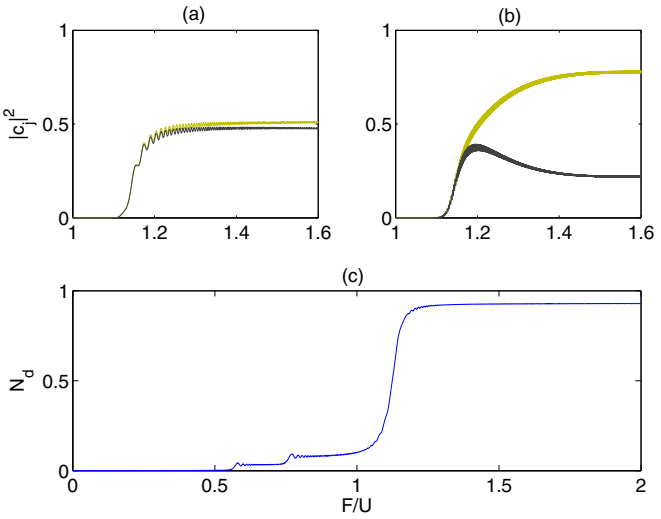

FIG. 9. Panels (a) and (b) show occupations of the correlated and uncorrelated DW states for the rates $\nu = 10^{-3}/2\pi$ and $\nu = 10^{-4}/2\pi$. (c) The mean number of doublons N_d normalized to $N_{\max} = L_x L_y/2$ as the function of time, where the time is related to F as $F = U\nu t$. Parameters are $J_y = 0.02U$, $J_x = 0.005U$, $L_x = 2$, $L_y = 4$, and $\nu = 10^{-3}/2\pi$.

The mean number of doublons, however, does not provide the whole information about the final state of the system—it can be only stated that populations of the correlated and uncorrelated DW states sum up to unity. For this reason we specifically address populations of the states Eqs. (19) and (20) [see Fig. 9(a)]. It appears that the chosen rate ν does not ensure a fully adiabatic regime, so that the populations of the correlated and uncorrelated DW states become almost equal due to the LZ tunneling between two lowest levels in Fig. 8(b). To obtain the correlated DW state as the final state the sweeping rate should be essentially smaller, smaller than the inverse gap (24). In fact, for $\nu = 10^{-4}/2\pi$ we already observe a misbalance in the population [see Fig. 9(b)], which tends to unity for smaller ν or, alternatively, larger J_x.

To conclude this section we comment on truncation of the Hilbert space to the doublon subspace. The validity of this approximation assumes a negligible population of the Fock states which may lead to triple occupations of the lattice sites. We have checked that during adiabatic passage the population of these states is of orders of magnitude smaller than the population of the resonant states. As the final check we repeated calculations shown in Fig. 9 by using the whole Hilbert space—the results appear to be almost identical. We stress, however, that the truncation of the whole Hilbert space to the doublon Hilbert space and further to the resonant subspace is justified only in the considered case of strong misalignment. If $\phi \approx 0$ we do observe a qualitative difference in the doublon dynamics when we truncate the Hilbert space.

VI. CONCLUSIONS

In the work we analyzed the evolution of the Mott-insulator state of cold atoms in 1D and 2D optical lattices as the lattices are tilted by applying a monotonically increasing static field $F = F(t)$. The analysis was performed by using the theory of multilevel Landau-Zener tunneling, properly adopted for the considered problem.

As concerns 1D lattices, the central result of the paper are Eqs. (9), (10), and (11), which give the number of produced doublons N_d as the function of the sweeping rate $\nu = dF/dt$. We paid particular attention to the adiabatic regime $\nu \to 0$, where the Mott-insulator state evolves into the density-wave state (empty lattice sites alternating with doublons). For this case we derived analytical expressions which capture the dynamics of the doublon number. It is shown that, having the goal to produce the density-wave state, one should use a protocol $F = F(t)$ which ensures diabatic transition of the multilevel avoided crossing at $F = U/2$, which is associated with the second-order tunneling, and adiabatic transition of the multilevel avoided crossing at $F = U$, associated with the first-order tunneling.

The above results are equally applied to the 2D square lattice, provided that the static field **F** is strongly mismatched with the primary axes of the lattice (for example, $1/3 < F_x/F_y < 1/2$). In this case the 2D lattices can be viewed as an array of weakly coupled 1D lattices. Correspondently, there are two adiabatic conditions for the rate ν. The first one is deduced from Eq. (10). It ensures that every column of the 2D lattice is a one-dimensional density-wave state. The second one requires $\nu \ll 1/\widetilde{\Delta}$, where $\widetilde{\Delta}$ is given in Eq. (22). It ensures that the column density waves are correlated; i.e., we have empty rows alternating with rows where every site has double occupancy.

It might be thought that the field orientation $\phi = \arctan(F_x/F_y) \approx 0$ is more suitable for producing the density-wave state in the square 2D lattice. This, however, is not the case. As shown in Ref. [34], for $\phi \approx 0$ the system has an intrinsic instability due to high mobility of the quasiparticles (doublons and holes) in the transverse x direction. For a strong misalignment this mobility is suppressed by the Wannier-Stark localization and the quasiparticles are essentially localized in the sites where they were created. Yet, a slightly larger than unity localization length introduces nonzero correlations in the x direction, which make it possible to produce the 2D density-wave state from the initial Mott-insulator state by means of the adiabatic passage.

ACKNOWLEDGMENTS

The authors acknowledge financial support from RFBR and KFN through Grant No. 16-42-240746. A.K. acknowledges fruitful discussions with F. Meinert and H.-Ch. Nägerl.

APPENDIX A

In this appendix we display explicit formulas for the dimension of the Hilbert spaces. The total dimension of the Hilbert space of the Bose-Hubbard model is given by the well-known equation

$$\mathcal{N} = \frac{(N+L-1)!}{(N-1)!L!}, \tag{A1}$$

where one should set $N = L$ in the case of unit filling. In the main text we refer to subspace of the total Hilbert space, which is defined by the condition $n_l \leqslant 2$, as the doublon Hilbert space. It has the dimension

$$\mathcal{N}_D = \sum_{n=0}^{L/2} \frac{L!}{(L-2n)!(n!)^2}. \tag{A2}$$

Finally, the dimension of the $j = 1$ resonant subspace is dependent on boundary conditions. For the open (Dirichlet) boundaries we have

$$\mathcal{N}'_R = \sum_{n=0}^{L/2} \frac{(L-n)!}{(L-2n)!n!}, \tag{A3}$$

while for the periodic boundary condition we have

$$\mathcal{N}_R = \mathcal{N}'_R(L) + \mathcal{N}'_R(L-2)\,. \tag{A4}$$

Needless to say that $\mathcal{N}_R < \mathcal{N}_D < \mathcal{N}$. For example, for $L = 8$ the inequality relation reads as $47 < 1107 < 6435$ and for $L = 16$ as $2207 < 519\,662\,7 < 300\,540\,195$. We also mention that in the case of the periodic boundary condition the dimension of every Hilbert space can be reduced by factor L if we take into account the conservation of the total quasimomentum.

APPENDIX B

To obtain a quantitative description of the second-order transition we consider the three-site Bose-Hubbard chain. Projecting Eq. (2) onto the basis vectors $|\psi_1\rangle = |1,1,1\rangle$, $|\psi_2\rangle = \frac{1}{\sqrt{3}}\sum_{l=0}^{2}\widehat{T}^l|0,2,1\rangle$, and $|\psi_3\rangle = \frac{1}{\sqrt{3}}\sum_{l=0}^{2}\widehat{T}^l|0,1,2\rangle$ (here $\widehat{T}$ is the cyclic permutation operator) and removing time dependance from the kinetic term through substitutions

$$\begin{aligned} |\psi_1\rangle &= e^{-i(Ut/2-\theta(t))}|\phi_1\rangle, \\ |\psi_2\rangle &= e^{-iUt/2}|\phi_2\rangle, \\ |\psi_3\rangle &= e^{-i(Ut/2+\theta(t))}|\phi_3\rangle, \end{aligned} \tag{B1}$$

we obtain

$$H(F) = \begin{pmatrix} -\mu(F) & -\frac{\sqrt{6}J}{2} & 0 \\ -\frac{\sqrt{6}J}{2} & \frac{U}{2} & -\frac{3J}{2} \\ 0 & -\frac{3J}{2} & \mu(F) \end{pmatrix}, \tag{B2}$$

where $\mu(F) = \frac{U}{2} - F$. The eigenvalues of this matrix could be found exactly by Cardano's formula. It is much simpler though to find an approximate solution for $\mu(F) \approx 0$ because we are only interested in the part of the spectrum underlying the second-order resonant transition. After some algebra we have

$$E_{1,2} = \frac{3J^2}{2U^2}\mu - \frac{15J^2}{4U} \mp \sqrt{\left(\frac{3J^2}{2U^2}\mu - \frac{15J^2}{4U}\right)^2 + \left(\mu^2 - \frac{3J^2}{2U}\mu\right)}$$

$$+O\left(\frac{J^2}{U^2}\right),$$

$$E_3 = \frac{U}{2} + O\left(\frac{J^2}{U^2}\right). \tag{B3}$$

The eigenvalues $E_{1,2}$, which show an avoided crossing at $\mu(F) \approx 0$, define the effective Hamiltonian. Basing on this effective Hamiltonian the mean number of doublons is given by

$$\frac{N_d(F)}{N_{\max}} \approx \frac{2}{3} \frac{\left((\mu - E_1)^2 + \frac{9J^2}{4}\right)(\mu + E_1)^2}{\left(\mu^2 - E_1^2\right)^2 + \frac{9J^2}{4}(\mu + E_1)^2 + \frac{3J^2}{2}(\mu - E_1)^2}. \tag{B4}$$

[1] M. Greiner, O. Mandel, T. Esslinger, T. W. Hänsch, and I. Bloch, Quantum phase transition from a superfluid to a Mott insulator in a gas of ultracold atoms, Nature (London) **415**, 39 (2002).

[2] S. Sachdev, K. Sengupta, and S. M. Girvin, Mott insulators in strong electric fields, Phys. Rev. B **66**, 075128 (2002).

[3] P. Fendley, K. Sengupta, and S. Sachdev, Competing density-wave orders in a one-dimensional hard-boson model, Phys. Rev. B **69**, 075106 (2004).

[4] K. Sengupta, S. Powell, and S. Sachdev, Quench dynamics across quantum critical points, Phys. Rev. A **69**, 053616 (2004).

[5] A. R. Kolovsky, Bloch oscillations in the Mott-insulator regime, Phys. Rev. A **70**, 015604 (2004).

[6] A. Polkovnikov, Universal adiabatic dynamics in the vicinity of a quantum critical point, Phys. Rev. B **72**, 161201(R) (2005).

[7] J. Simon, W. S. Bakr, R. Ma, M. E. Tai, P. M. Preiss, and M. Greiner, Quantum simulation of antiferromagnetic spin chains in an optical lattices, Nature (London) **472**, 307 (2011).

[8] F. Meinert, M. J. Mark, E. Kirilov, K. Lauber, P. Weinmann, A. J. Daley, and H.-C. Nägerl, Quantum Quench in an Atomic One-Dimensional Ising Chain, Phys. Rev. Lett. **111**, 053003 (2013).

[9] I. B. Spielman, Atomic physics: A route to quantum magnetism, Nature (London) **472**, 301 (2011).

[10] M. Eckstein and Ph. Werner, Dielectric breakdown of Mott insulators: Doublon production and doublon heating, J. Phys.: Conf. Ser. **427**, 012005 (2013).

[11] T. Oka, Nonlinear doublon production in a Mott insulator: Landau-Dykhne method applied to an integrable model, Phys. Rev. B **86**, 075148 (2012).

[12] E. Lundh, Mott-insulator dynamics, Phys. Rev. A **84**, 033603 (2011).

[13] R. Ma, M. E. Tai, Ph. M. Preiss, W. S. Bakr, J. Simon, and M. Greiner, Photon-Assisted Tunneling in a Biased Strongly Correlated Bose Gas, Phys. Rev. Lett. **107**, 095301 (2011).

[14] K. Balzer and M. Eckstein, Field-assisted doublon manipulation in the Hubbard model: A quantum doublon ratchet, Europhys. Lett. **107**, 57012 (2014).

[15] C. P. Rubbo, S. R. Manmana, B. M. Peden, M. J. Holland, and A. M. Rey, Resonantly enhanced tunneling and transport of ultracold atoms on tilted optical lattices, Phys. Rev. A **84**, 033638 (2011).

[16] K. W. Mahmud, L. Jiang, E. Tiesinga, and P. R. Johnson, Bloch oscillations and quench dynamics of interacting bosons in an optical lattice, Phys. Rev. A **89**, 023606 (2014).

[17] Zi Cai, Lei Wang, X. C. Xie, and Yupeng Wang, Interaction-induced anomalous transport behavior in one-dimensional optical lattices, Phys. Rev. A **81**, 043602 (2010).

[18] F. Meinert, M. J. Mark, E. Kirilov, K. Lauber, P. Weinmann, M. Gröbner, A. J. Daley, and H.-Ch. Nägerl, Observation of many-body long-range tunneling after a quantum quench, Science **344**, 1259 (2014).

[19] F. Queisser, P. Navez, and R. Schützhold, Sauter-Schwinger-like tunneling in tilted Bose-Hubbard lattices in the Mott phase, Phys. Rev. A **85**, 033625 (2012).

[20] M. H. Muñoz-Arias, J. Madroñero, and C. A. Parra-Murillo, Off-resonant many-body quantum carpets in strongly tilted optical lattices, Phys. Rev. A **93**, 043603 (2016).

[21] S. Pielawa, T. Kitagawa, E. Berg, and S. Sachdev, Correlated phases of bosons in tilted frustrated lattices, Phys. Rev. B **83**, 205135 (2011).

[22] S. Pielawa, E. Berg, and S. Sachdev, Frustrated quantum Ising spins simulated by spinless bosons in a tilted lattice: From a quantum liquid to antiferromagnetic order, Phys. Rev. B **86**, 184435 (2012).

[23] M. Kolodrubetz, B. K. Clark, and D. A. Huse, Nonequilibrium Dynamic Critical Scaling of the Quantum Ising Chain, Phys. Rev. Lett. **109**, 015701 (2012).

[24] M. Kolodrubetz, D. Pekker, B. K. Clark, and K. Sengupta, Nonequilibrium dynamics of bosonic Mott insulators in an electric field, Phys. Rev. B **85**, 100505(R) (2012).

[25] A. J. Daley, M. Rigol, and D. S. Weiss, Focus on out-of-equilibrium dynamics in strongly interacting one-dimensional systems, New J. Phys. **16**, 095006 (2014).

[26] C. A. Parra-Murilloa, J. Madroñero, and S. Wimberger, Exact numerical methods for a many-body WannierStark system, Comput. Phys. Commun. **186**, 19 (2014).

[27] V. L. Pokrovsky and N. A. Sinitsyn, Landau-Zener transitions in a linear chain, Phys. Rev. B **65**, 153105 (2002).

[28] V. N. Ostrovsky and M. V. Volkov, Landau-Zener transitions in a system of interacting spins: Exact results for demagnetization probability, Phys. Rev. B **73**, 060405(R) (2006).

[29] N. A. Sinitsyn, Landau-Zener transitions in chains, Phys. Rev. A **87**, 032701 (2013).

[30] A. V. Shytov, Landau-zener transitions in a multilevel system: An exact result, Phys. Rev. A **70**, 052708 (2004).

[31] A. Tomadin, R. Mannella, and S. Wimberger, Many-body Landau-Zener tunneling in the Bose-Hubbard model, Phys. Rev. A **77**, 013606 (2008).

[32] When simulating the system dynamics in the whole Hilbert space it is important to take into account corrections to the interaction energy of the triply (and higher) occupied sites [33]. In many cases this rejustified the broken doublon approximation.

[33] M. J. Mark, E. Haller, K. Lauber, J. G. Danzl, A. Janisch, H. P. Büchler, A. J. Daley, and H.-C. Nägerl, Preparation and Spectroscopy of a Metastable Mott-Insulator State with Attractive Interactions, Phys. Rev. Lett. **108**, 215302 (2012).

[34] A. R. Kolovsky, Quantum phase transitions in two-dimensional tilted optical lattices, Phys. Rev. A **93**, 033626 (2016).